Excellent charts and references. Good reading!

LAWRENCE
LIVERMORE
NATIONAL
LABORATORY

LLNL-TR-692694

Role of Off-Line-of-Sight Propagation in Geomagnetic EMP Formation

H. W. Kruger

May 23, 2016

Disclaimer

This work performed under the auspices of the U.S. Department of Energy by Lawrence Livermore National Laboratory under Contract DE-AC52-07NA27344.

Role of Off-Line-of-Sight Propagation in Geomagnetic EMP Formation

Hans Kruger

Lawrence Livermore National Laboratory

Abstract

The author's synchrotron radiation based 3D geomagnetic EMP code MACSYNC has been used to explore the impact on pulse rise time and air conductivity of EMP propagation paths to the observer that are located off the direct line-of-sight (LOS) between gamma source and observer. This geometry is always present because, for an isotropic source, most the gammas are emitted at an angle with respect to the LOS. Computations for a 1 kt near-surface burst observed from space yield two principal findings:

1. The rise time is generated by the combined actions of a) electron spreading along the LOS due to the Compton electron emission angular distribution folded with electron multiple scattering effects, and b) radiation arrival time spreading due to length differences for different off-LOS propagation paths. The pulse rise time does not depend on the rise time of the conductivity. The conductivity rise time determines the pulse amplitude.
2. One-dimensional legacy EMP codes are inherently incapable of producing the correct pulse shape because they cannot treat the dependence of the conductivity on two dimensions, i.e. the radius from the source and the angle of the propagation path with the LOS. This divergence from one-dimensionality begins at a small fraction of a nanosecond for a sea-level burst. This effect will also be present in high-altitude bursts, however, determination of its onset time and magnitude requires high-altitude computations which have not yet been done.

Introduction

In previous papers, the author discussed the effect on the later part of a geomagnetic EM pulse due to conduction electron attachment during the delay between ionization creation and EMP arrival caused by the flight path difference between the ionizing gammas and the EMP for off-line-of-sight (LOS) propagation paths [1-3]. The current paper deals with the wider role of off-LOS propagation in the formation of geomagnetic EM pulses with emphasis on pulses from low-yield, near-surface explosions observed

from space. This is another progress report on the author's exploration of the impact of a fully three-dimensional treatment on the computed geomagnetic EMP.

The current paper is based on calculations with the author's 3D MACSYNC geomagnetic EMP code described in Reference 1.

About MACSYNC

The author developed MACSYNC as a tool to explore the impact on geomagnetic EMP computations of 3D effects that cannot be treated by the commonly used one-dimensional legacy codes. The main purpose of MACSYNC computations has always been to motivate the development by others of 3D codes solving Maxwell's equations. MACSYNC was never intended to become a general production tool for precise geomagnetic EMP computations.

MACSYNC uses LANL's three-dimensional coupled gamma-electron transport code MCNP as a subroutine providing electron position and velocity vector information to its EMP generation and propagation routines [4]. MCNP chooses an electron transport step based on the percent of energy loss per spatial step which is a user input. The maximum energy loss per major step that MNP allows is 8% of the instantaneous energy, because MCNP updates the electron's transport properties after such an energy loss. The user specifies the number of substeps per major step. The author used 20 substeps for the current calculations corresponding to ~5 cm per step for 3 Mev electrons. For each of these transport steps, MACSYNC calculates the EMP radiated in the direction of the observer using the instantaneous direction of the velocity vector, i.e. the angle between the synchrotron radiation beacon and the radius vector to the observer at the end of each transport step. This field is then attenuated on its path to the observer, in 10 meter steps between the source and a radius of 2 km, through the conductivity present at each of these EMP propagation steps at the moment of EMP arrival at that step.

The EMP attenuation method used in MACSYNC assumes that the EM propagation through ionized air caused by the nuclear explosion is pure attenuation, i.e. frequency independent. This is the case for the collision-dominated plasma surrounding sea level and low-altitude bursts observed from space. It is also so for high-altitude bursts observed on the ground as long as the yield is large enough so that radiation from electrons at higher altitudes is fully attenuated and only radiation originating at lower altitudes can penetrate to the ground. EM propagation from electrons radiating above ~30 km altitude to the ground is somewhat frequency dependent.

In MCNP, neither the EMP propagation nor the electron transport use any fixed cells. The gamma transport uses spherical shells, chosen 100 m thick, for gamma splitting as a gamma crosses from one shell into another. This is a standard Monte Carlo technique for keeping the number of transported gammas high for problems, like the current EMP problem, involving deep penetration over many gamma interaction mean-free-paths. These MCNP shells are also used by MACSYNC to identify the shell within which the

EMP reaching the observer originated. For each shell, MACSYNC tallies the EMP vs. time of arrival at the observer using five dozen adjacent time intervals distributed approximately uniformly over a logarithmic time axis, with approximately ten time bins per decade over six decades from 0.001 to 1000 shakes. (One shake, equaling ten nanoseconds, is the unit of time used in MCNP.) The total EMP at the observer is obtained at the end of the MACSYNC run by adding the contributions from all the shells.

In the MACSYNC calculations discussed in this paper, the z-axis points at the observer and the earth's magnetic field points along the y-axis. For this geometry, MACSYNC calculates only the x-, i.e. in-plane, component of the EMP since the y-component cancels for an isotropic gamma source in a uniform air environment.

The conductivity model used in the MACSYNC calculations for ground burst scenarios reported in References 1-3 made the approximation of immediate energy deposition by the Compton electrons. It also ignored the formative time lag because this process is negligibly short at sea level air densities [5]. It used an electron mobility of 0.3 m/s per V/m and an electron attachment time constant of 1 shake = 10 nanoseconds, the two nominal values used by Conrad Longmire in his IEEE paper [6].

Separate time-dependent energy depositions by unscattered or scattered gammas used in the conductivity model of References 1-3 were obtained with MCNP calculations. Conduction electron attachment effects were included. The resultant conductivity due to conduction electrons or ions is shown in Fig. 1 at selected radii from the burst point. The model includes a linear conductivity ramp that can be used to model the effect of a gamma pulse width or of a finite Compton electron energy deposition time. The conductivity ramp used for Fig. 1 was 0.1 shakes.

For the calculations to be discussed in this paper, a detailed time-dependent energy deposition by the Compton electron was added as an option to this conductivity model (thanks to LLNL's Chester Eng for encouraging the author to make this improvement). The energy deposition was obtained from MCNP calculations using time-dependent transport of both gammas and electrons. The energy deposition was tallied as a function of time in a 10 cm thick spherical shell of air located at 1 km from a line source of 3 Mev gammas. A 20 meter thick buffer shell of air was adjacent to both sides of the tally shell. This thickness was chosen on the basis of two considerations. On the one hand, it should be as thin as possible to minimize gamma scattering which would artificially lengthen the apparent electron energy deposition time. On the other hand, it needed to be to be larger than the range of the maximum-energy Compton electron produced by 3 Mev gammas, so that all Compton electrons made within their range from the tally shell, on either side of the tally shell, would be able to reach it. The volume between the source and the inner buffer shell was a vacuum to avoid gamma scattering.

Two sets of MCNP calculations were run (see Fig. 2). In one set, gammas and electrons were prevented from crossing the downstream surface of the tally shell, while in the second set they were allowed to cross this surface. The second set calculated a somewhat higher energy deposition due to electrons scattering back into the tally shell from the downstream buffer shell. The energy density versus time from this second set of calculations was chosen for the conductivity model because it more accurately

represents the transport physics. It is shown in normalized form in Fig. 3. The normalized ion density is identical to the normalized energy density because there is no appreciable ion attachment on time scales of interest. However, the normalized conduction electron density follows the normalized energy density only initially, but then peaks and falls off because of conduction electron attachment to neutrals. This is also shown in Fig. 3.

The EMP propagation geometry for gammas emitted at an angle theta with the LOS to a distant observer, such as a space-based detector, is depicted in Fig. 4. At the time the EMP, emitted at a point located at a radius R and angle theta with the LOS, reaches a volume element located at a radius R+dR, the ionization density, created in that volume element by gammas reaching it by a direct and thus shorter path, has decreased due conduction electron attachment. This delay between the arrivals of the ionizing gammas and the EMP, that allows attachment, is plotted as a function of theta in Fig.5 for R=1000 m and dR=500 m. This value of R+dR was chosen because it is a location from which propagation to a distant observer is neither negligible nor 100% for a 1 kt burst as will be shown in a following section. It can be seen that this delay can be of the order of one attachment time, 1 sh or 10 nanoseconds, for theta ~8 degrees. The corresponding arrival time at the observer, also plotted in Fig.5, is ~30 nanoseconds. For later observer times, i.e. larger theta angles, the delay time available for attachment rapidly increases, as can be seen from Fig. 5.

The effect of conduction electron attachment, due to off-LOS propagation, on the MACSYNC conductivity models will be shown in the following few Figures. In Fig. 6, the conductivity contributions from unscattered gammas, scattered gammas or ions, as well as the total conductivity, are plotted at an 800 m radius for the ramped conductivity model, using a 0.01 sh ramp, and the new conductivity model based on the detailed time dependent Compton electron transport calculations. The conductivity is shown as a function of time after arrival of the first gamma at that radius. In Fig. 7, the total conductivity is plotted versus the same time, also at an 800 m radius, for the ramped conductivity model for 0.01, 0.1, 0.5, and 1 sh ramps, as well as for the time-dependent electron transport (TDET) conductivity model. It can be seen that the models differ only in the time over which the conductivity reaches its peak, while the decrease in conductivity at later times is similar for all of them. It can also be noted that the TDET model and the ramped model, using a 0.5 sh ramp, provide very similar conductivity vs. time profiles.

The next two Figures summarize differences in conductivity time histories, due to off-LOS propagation at different theta angles, following EMP arrival at a radius of 1500 m. Again this radius was chosen because it is in the semi-transparent region between the EMP-opaque and EMP-transparent regions. Fig. 8 shows the on-LOS conductivity for the TDET model with arrows marking the EMP arrival time for various theta off-LOS emission angles taken from Fig. 5. These conductivities for various off-LOS theta angles are overlaid in Fig. 9 using the time of EMP arrival at 1500 m as a common time axis origin. It can be seen from this Figure that the conductivity, at a given time after EMP arrival, can vary by more than an order-of-magnitude between on-LOS and off-LOS propagation paths.

Both the ramped and the TDET conductivity models will be used in the remainder of the paper to examine the role of off-LOS propagation in geomagnetic EM pulse rise time formation and pulse shape.

Conductivity due to air ionization by preceding bursts was not an issue because the low yield used in these calculations was produced by a single-stage nuclear device. Pre-ionization of the air by the x-rays accompanying the gammas was considered by not including, in the total radiated field, contributions from electrons located within the first 100 m tally radius. These contributions were negligibly small, even in the absence of x-ray ionization, because of the steep increase in ionization density with decreasing radius caused by the radius-squared dependence of the gamma fluence.

The deceleration, or drag, of the electron due to collisions with air does not produce any net radiated field for an isotropic source in a symmetric geometry. However, in most burst environments there exist asymmetries due to such factors as an air-ground interface and an air or humidity density gradient. This asymmetric drag EMP needs to be added to the geomagnetic EMP. However, LANL's Bill Clodius and MRC's Bill Crevier and Bob Hamilton have shown, using AFWL's SCX or MRC's AGRIP and LEMP codes, respectively, that the asymmetric drag EMP produced in surface or near-surface bursts, viz. the geometry of interest to this paper, is much smaller than the geomagnetic EMP, and has a much longer rise time, for all viewing angles larger than approximately half-a-dozen degrees relative to the earth horizon [7,8]. Thus asymmetric drag EMP is not an issue for this paper since most satellites, which could be used for EMP detection, are at larger elevation angles and since its longer rise time is less capable of penetrating the ionosphere on the way to the satellite.

Off-LOS propagation and conductivity ramp effects on rise time

The ramped conductivity model with a 0.5 sh ramp has been used in a series of MACSYNC calculations to explore the role of off-LOS propagation in pulse rise time formation. All calculations used a total yield of 1 kt, a 0.3% gamma yield fraction, a gamma energy of 3 Mev, a 0.01 sh wide pedestal gamma output pulse, and a 0.5 gauss magnetic field.

The first series of a dozen calculations used 0.1 degree wide gamma emission bands. The first calculation used theta between 0 and 0.1 degrees, the second calculation used theta between 0.1 and 0.2 degrees, the third theta between 0.2 and 0.3 degrees, etc. The field computed for theta=0-0.1 degrees is shown in Fig. 10. It rises to a peak in a time approximately equal to the gamma pulse width. After the peak, the field drops with a long tail extending well beyond the 0.2 sh shown on the Figure. This tail is caused by the spreading of the radiating electrons along the LOS due to the Klein-Nishima Compton electron emission angular distribution folded with electron multiple scattering effects.

The fields from the entire series of 0.1 degree wide gamma emission bands is shown in Fig. 11 along with their sum. It can be seen that the rise is produced by these pulses as

they arrive with increasing delays due to the longer path lengths associated with off-LOS propagation at increasing angles with the LOS. The early-arriving pulses have a lower amplitude because the number of gammas emitted into their smaller fractional solid angle is smaller than that of later-arriving pulses (see Fig. 12).

The entire pulse is produced in a second series of a dozen calculations with increasing emission angle widths of 0-0.1, 0.1-0.2, 0.2-0.4, 0.4-0.8, 0.8-1.6, 1.6-3.2,3.2-6.4, 6.4-12.8, 12.8-25.6, 25.6-51.2, 51.2-102.4, and 102.4-180 degrees. This series of calculations was done with the ramped conductivity model using either 0.01, 0.1, 0.5, or 1 sh ramps (see Figs. 13-16). The same series of calculations was also done with the TDET conductivity model (see Fig. 17). The sums of fields of the angular emission bands for the different conductivity ramps are overlaid in Fig. 18 along with the sum of fields for the TDET conductivity model. It can be seen that the calculations with the 0.5 sh ramp and the TDET conductivity models give similar fields, as expected based on their similar conductivity vs. time profiles. It is also noted that the pulse rise times are approximately the same for all the ramps and thus do not depend on the conductivity rise time.

Figs. 19-22 show the contributions of the different 100 m thick air shells to the total fields shown in Figs. 13-16 of the preceding paragraph. It can be seen that the effect of a shorter conductivity ramp is to reduce the contribution of inner air shells to the total pulse at earlier times by increasing the conductivity faster. This results in a “black-out” at early times of the EMP generated in the inner shells. This black-out effect is evident in Fig. 23 which shows the EMP transmission to a distant observer from radiating electrons located at a given radius from the source. This transmission is plotted for various percentages of the final conductivity along the linear conductivity ramp. The Figure also plots the transmission for 100% conductivity, for various delay times after completion of the ramp rise when attachment has reduced the conductivity.

In summary, the rise time of the geomagnetic pulse is due to the combined effects of a) electron spreading along the LOS due to the Compton electron emission angular distribution folded with multiple scattering effects, and b) radiation arrival time spreading due to path length differences for different off-LOS gamma emission angles. The pulse rise time does not depend on the rise time of the conductivity. The conductivity rise time determines what part of the source volume is EM-opaque and not visible to the observer. This determines the amplitude of the pulse.

Three-dimensional conductivity effect on pulse shape

The preceding paragraphs show that the conductivity time profile experienced by the EMP does not depend alone on the radial distance from the source, but also on the particular off-LOS propagation path traveled by the EMP. In other words, the conductivity is a function not of one but of all three dimensions.

The legacy EMP codes, HEMP and CHAP, are one-dimensional. They can treat the conductivity only as a function of the radius. The next few Figures compare the field

computed by MACSYNC using a fully three-dimensional conductivity with the same MACSYNC problem run with a conductivity depending only on the radiating electron's radius.

Both problems used the ramp conductivity model with a 0.5 sh ramp. Fig.24 shows the fields generated in all the spherical air shells for the standard three-dimensional conductivity treatment. Fig. 25 shows the same fields when the delay due to off-LOS propagation of the gammas has been removed from the time determining the conductivity, viz. the conductivity is the theta=zero degrees conductivity shown in Fig. 8. Comparison of these two Figures shows that radiation originating in the inner shells is cut off early by the 3D conductivity, while this is not the case for the 1D conductivity.

Fig. 26 shows the total field for the 1D conductivity model. In Fig.27 the total fields computed with the 1D and 3D conductivity models are overlaid. It is evident from this Figure that a 1D conductivity produces a significantly different pulse shape than the fully 3D conductivity treatment. The two treatments track one another during the early rise of the pulse. Then the 1D treatment produces a substantially larger field until, near the end of the pulse, it generates a smaller field than the 3D treatment. These differences in computed fields are consistent with expectation based on comparing the conductivity vs. time of the two treatments shown in Fig. 9.

In summary, it is evident that one-dimensional EMP codes are inherently incapable of producing the correct geomagnetic EMP shape, in a sea level burst geometry, because they cannot treat the dependence of conductivity on two dimensions, viz. radius and angle with the LOS.

Discussion

Farmer, et al., recently arrived at findings that seem to be inconsistent with the principal findings of this paper. They found that: 1. Legacy 1D (spherical) EMP codes contain the off-LOS propagation effects because they are included in the Maxwell equations solved by those codes [9], and 2. Temporal evolution of the conductivity is the biggest factor in determining the EMP rise time, with the precise temporal form of the gamma pulse and any pre-ionization of the atmosphere having a greater influence on the pulse shape than use of the obliquity-factor scattering treatment or off-LOS propagation effects beyond those captured in a CHAP-like model [9,10]. Three-dimensional effects were outside the scope of the work by Farmer et al, and for that reason they limited themselves to a one-dimensional (spherically symmetric) model of the conductivity. The current paper treats the behavior at longer times for which the off-LOS propagation effects are more important, requiring a multi-dimensional description. At the high altitudes of the scenario treated by Farmer et al, the conduction electron attachment times are very long, allowing ionization from previous bursts to persist for long times. If such pre-ionization had been included in their calculations, the leading edge of the pulse would have been attenuated, producing a different temporal profile. The impact of such pre-ionization is consistent with their conclusion that the temporal evolution of the conductivity is a

dominant effect on the formation of the EMP, though a detailed description of these effects was also outside the scope of their work.

The current paper treats 3D conductivity for near-surface bursts observed from space. In high-altitude bursts observed from the ground, the gamma emission angle associated with a given observer time is typically an order-of-magnitude smaller than the same angle in a ground burst. The author has found, however, that the delay time between ionization creation and EMP arrival is roughly the same fraction of the observer time for both burst scenarios. Thus 3D conductivity effects will also be an issue for high-altitude bursts. The conductivity vs. time profile is determined at early times by the Compton electron energy deposition time and at late times by the conduction electron attachment time. The first scales inversely with air density, while the second scales approximately inversely with air density or its square depending on whether two-body or three-body attachment dominates at a given altitude . Thus the high-altitude burst conductivity vs. time profile will vary with the altitude of the radiating electron, which determines the altitudes traversed by the EMP on its path to the observer, and it will be different from a near-surface burst profile. The magnitude of the 3D conductivity effect for high-altitude bursts depends on the details of the conductivity profile. The author has not yet built a high-altitude version of MACSYNC capable of investigating the resulting impact of 3D conductivity on pulse shape for this high-altitude burst geometry.

A few years ago, Chester Eng suggested to the author Compton electron deflection by the earth's magnetic field as another asymmetry mechanism producing a net drag EMP. This possibility has recently been explored by Friedman et al [11]. Using a simplified high-altitude geometry consisting of electron or gamma sources radiating into a uniform slab of unionized air with a density corresponding to that at 20 km, they found a noticeable effect. This issue deserves more detailed modelling with isotropic gamma sources, including air conductivity and pre-ionization, for near-surface and high-altitude bursts in order to find out how this effect compares to geomagnetic EMP and the other asymmetry drag EMP mechanisms for various viewing geometries. If this modelling shows the new asymmetric drag EMP to be significant, then the legacy asymmetry drag EMP codes, SCX, AGRIP, and LEMP, which do not use the earth's magnetic field in their calculations, ought to be updated.

Conclusions and observations

The MACSYNC calculations discussed in this paper lead the author to the following conclusions for near-surface bursts observed from space:

1. The rise time of the geomagnetic pulse is due to the combined actions of
   a) electron spreading along the LOS due to the Compton electron emission angular distribution folded with electron multiple scattering effects, and
   b) radiation arrival time spreading due to length differences for different off-LOS propagation paths. The pulse rise time does not depend on the rise time of the conductivity.

2. One-dimensional legacy EMP codes are inherently incapable of producing the correct geomagnetic EMP shape because they cannot treat the dependence of the conductivity on two dimensions, i.e. the radius from the source and the angle of the propagation path with the LOS.

The same phenomenology occurs in high-altitude bursts observed from the ground. In order to assess the degree to which this actually affects the geomagnetic EMP rise time and general shape in this burst environment, the author would need to build a high-altitude version of MACSYNC. The current development of a 3D Maxwell's equation solver at LLNL, led by David Larson, will also be able to address this high-altitude burst issue.

Acknowledgement

The author is indebted to LLNL's EMP code development team (Bruce Cohen, Chester Eng, Will Farmer, Alex Friedman, David Grote, and David Larson) whose stimulating discussions with him motivated this paper. He also appreciates technical support from LANL's MCNP team members Tim Goorley and Grady Hughes.

References

1. H. Kruger, "3D Effects in Geomagnetic EMP Computations", J. Radiation Effects, Research and Engineering, vol. 31, No. 1, p.159 (2013).
2. H. Kruger, "Gamma Shadow Effects on Geomagnetic EMP Rise Time and Amplitude", J. Radiation Effects, Research and Engineering, vol. 33, No. 1, p. 13 (2015).
3. H. Kruger, "Geomagnetic EMP Sources Radiating through a Gamma Shadow", J. Radiation Effects, Research and Engineering, vol. 33, No. 1, p. 1 (2015).
4. Los Alamos National Laboratory X-5 Monte Carlo Team, "MCNP – A General Monte Carlo N-Particle Transport Code, Version 5", LA-UR-03-1987, 2005.
5. C. L. Longmire and J. Koppel, "Formative Time Lag of Secondary Ionization", MRC-R-88, January 1974.
6. C. L. Longmire, "On the Electromagnetic Pulse Produced by Nuclear Explosions", IEEE Trans. On Antennas and Propagation, vol. AP-26, No. 1, p. 3 (1978).
7. William B. Clodius, "Radiated Surface Burst VHF EMP for Selected Devices (U)", LA-11946-MS, Aug. 19, 1990, and "Radiated Low Altitude VHF Geomagnetic EMP for Selected Devices (U)", LA-12053-MS, May 13, 1991.
8. R. M. Hamilton and W. F. Crevier, "EMP Generation by Potential Fission or Fusion Defensive Warheads (U)", UCRL-15485 (1985).

9. W. A. Farmer, B. I. Cohen, and C. D. Eng, “Assessing the validity of common approximations used in modeling nuclear EMP”, LLNL-PRES-683958 (2016), presentation at 2016 Hardened Electronics and Radiation Technology (HEART) Conference, April 7, 2016.
10. W. A. Farmer, B. I. Cohen, and C. D. Eng, “On the validity of certain approximations used in the modeling of nuclear EMP”, IEEE Trans. Nucl. Sci., vol. 63, No. 2, p. 1259 (2015).
11. A. Friedman, W. A. Farmer, B. I. Cohen, C. D. Eng, D. P. Grote, H. W. Kruger, and D. J. Larson, “Studies of EMP Generation using a Lienard-Wiechert Formulation, and Progress toward a 3-D EMP Code”, accepted for publication in J. Radiation Effects, Research and Engineering, 2016.

Figures

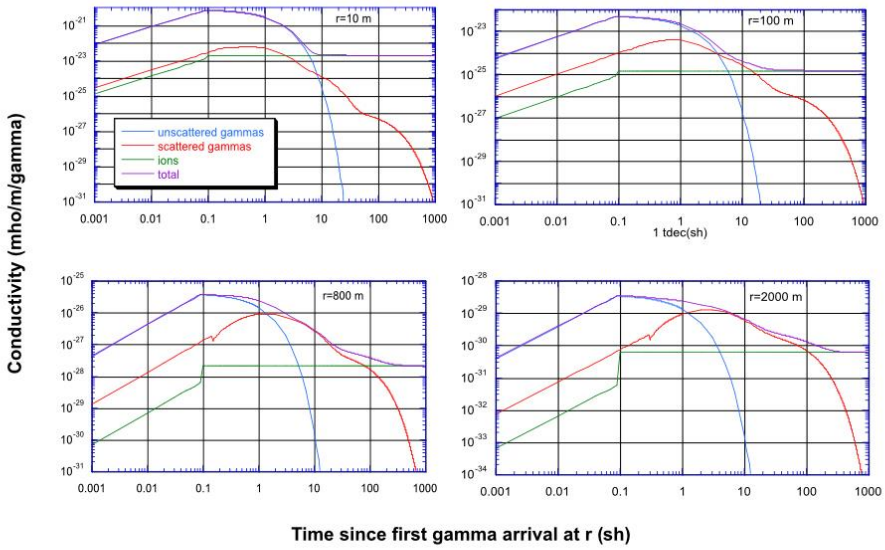

Figure 1. Conductivity using a 0.1 shake ramp.

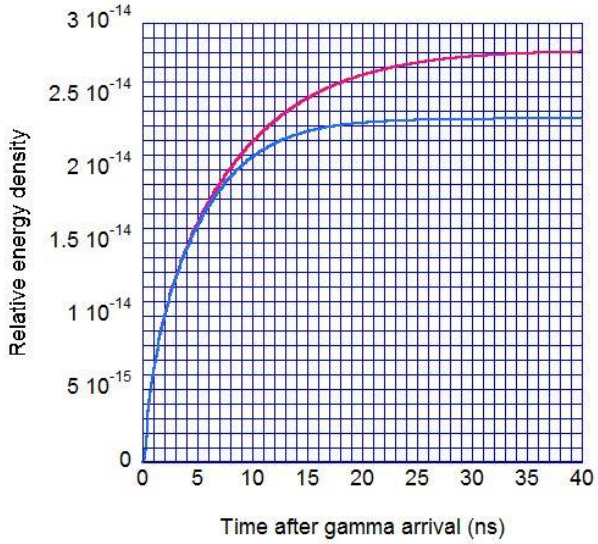

Figure 2. Compton electron energy deposition vs. time in sea level air for 3 Mev gammas. Upper curve includes electron back scattering, the lower one does not.

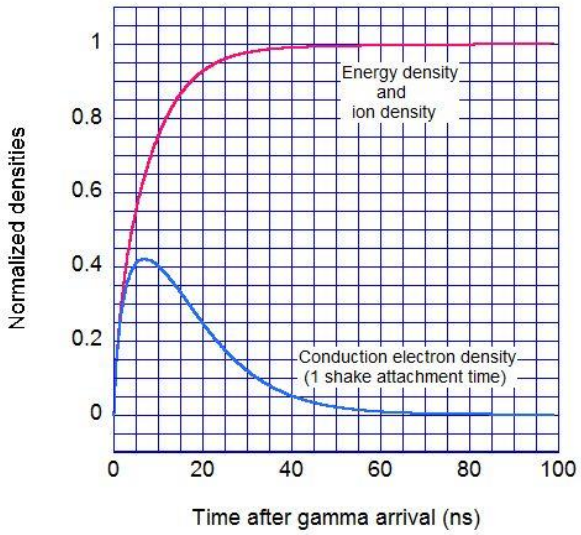

Figure 3. Conduction electron and ion density vs. time in sea level air for 3 Mev gammas.

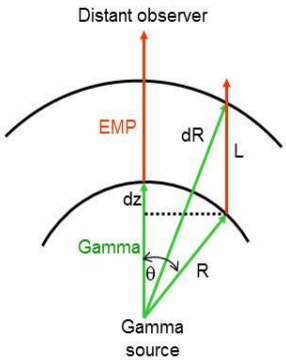

Figure 4. EMP propagation geometry to a distant observer for gammas emitted at an angle theta with the line-of-sight (LOS).

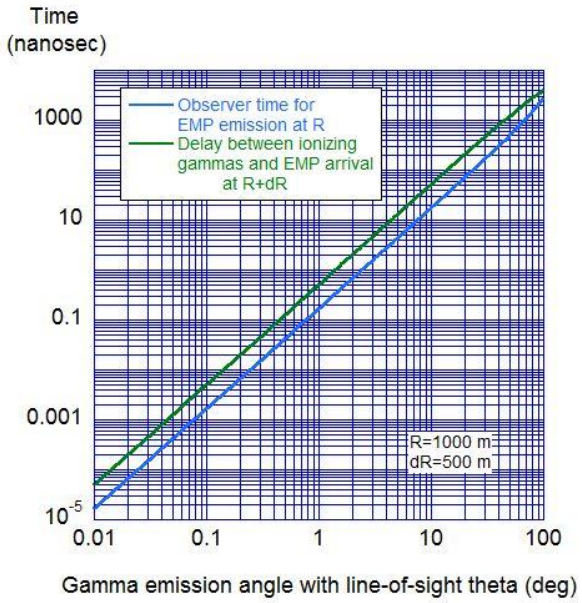

Figure 5. Observer and delay times for EMP, emitted at a point located at R=1000 m and angle theta with the LOS, when reaching a volume element of ionized air at R+dR=1500 m.

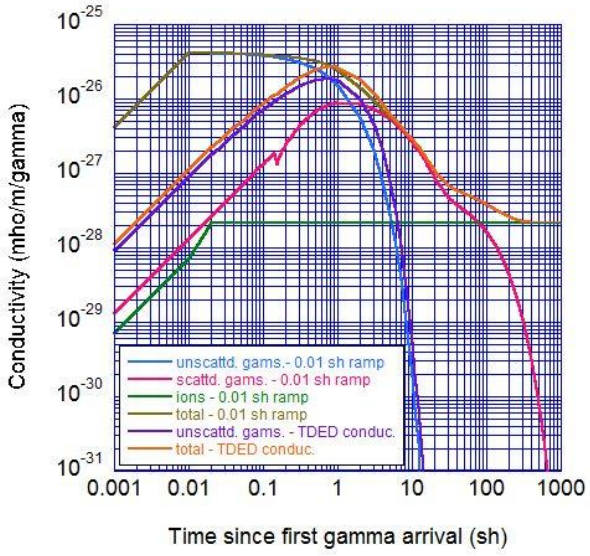

Figure 6. Conductivity contributions from unscattered or scattered gammas and ions at 800 m for 1 kt total yield, 0.3% gamma yield and a gamma energy of 3 Mev.

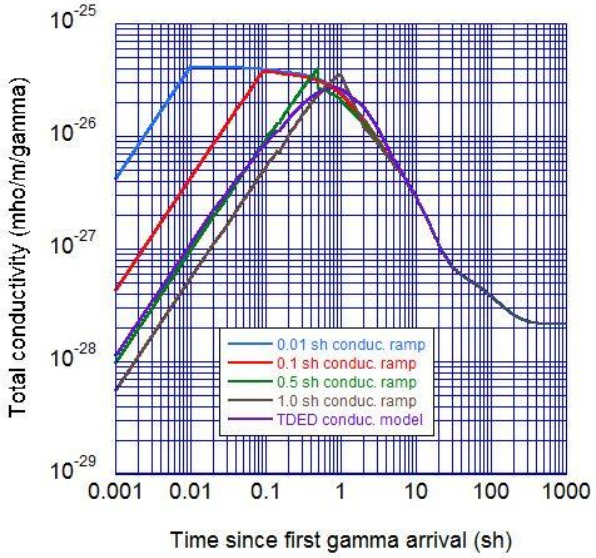

Figure 7. Total conductivity at 800 m for the ramped conductivity and the time-dependent electron transport (TDET) models.

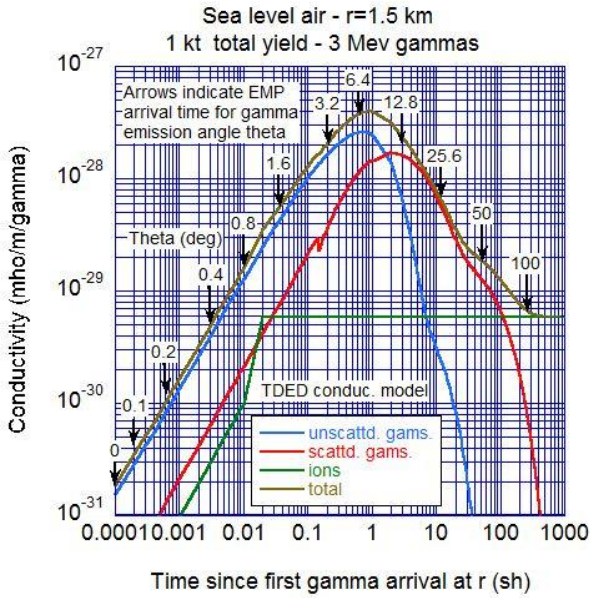

Figure 8. On-LOS conductivity, from the TDET conductivity model, at 1.5 km. Arrows mark the EMP arrival time for various gamma emission angles.

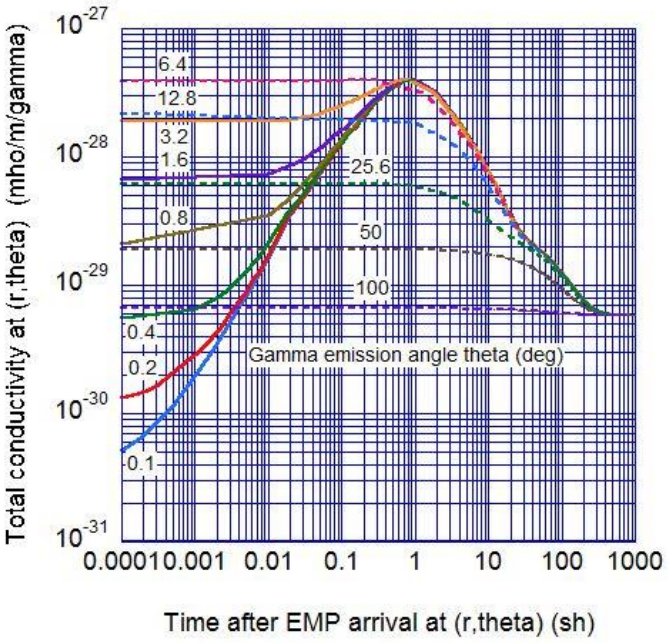

Figure 9. Conductivity at 1500 m for various gamma emission angles.

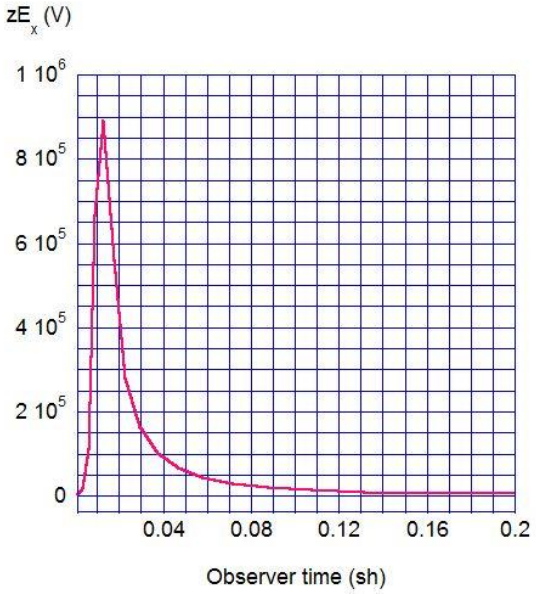

Figure 10. Field for gammas emitted between 0 and 0.1 degrees with the LOS. Total yield 1 kt, 0.3% gamma yield with 3 Mev gamma energy.

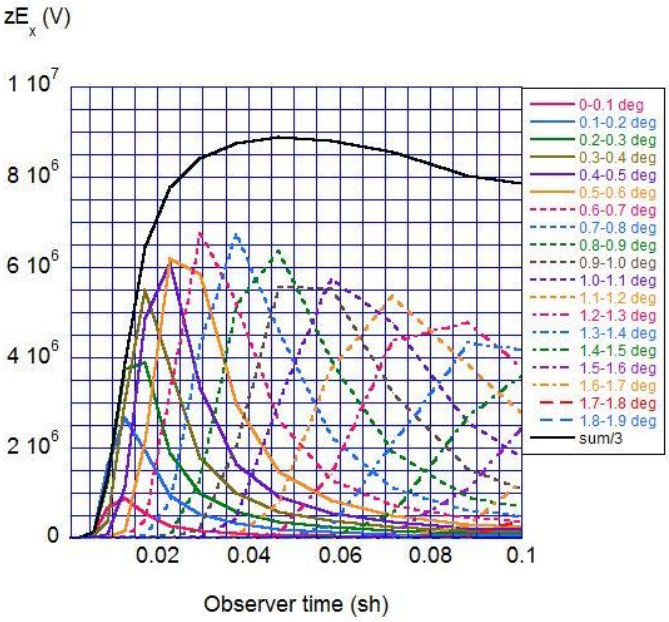

Figure 11. Field from gammas emitted into indicated adjacent 0.1 degree wide emission angle bands.

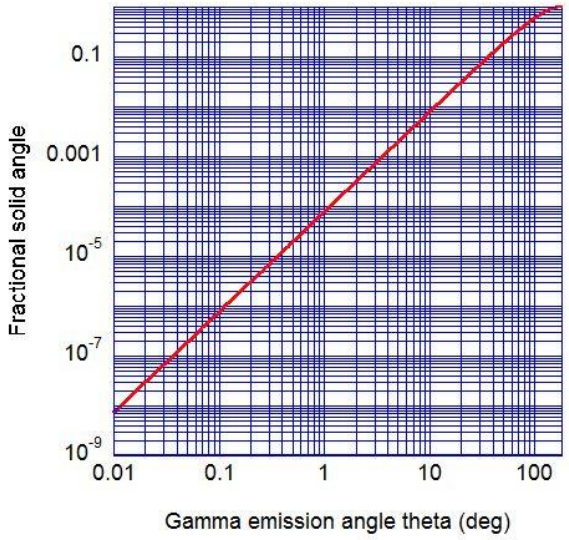

Figure 12. Fractional solid angle for gammas emitted into an angle theta with the LOS.

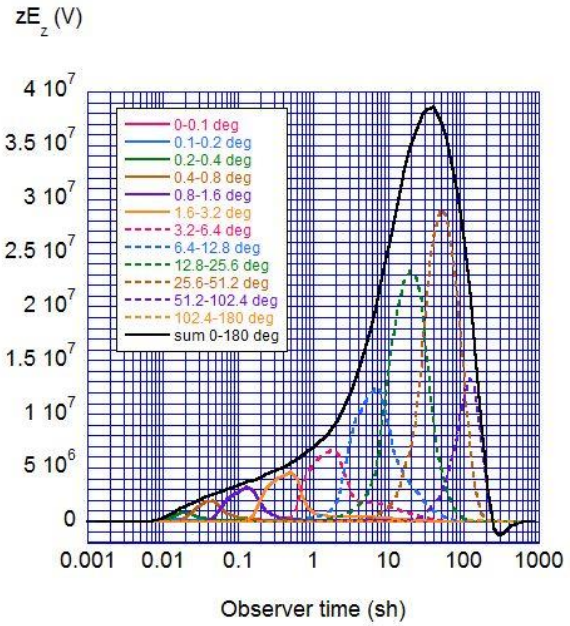

Figure 13. Field for a 0.01 sh conductivity ramp.

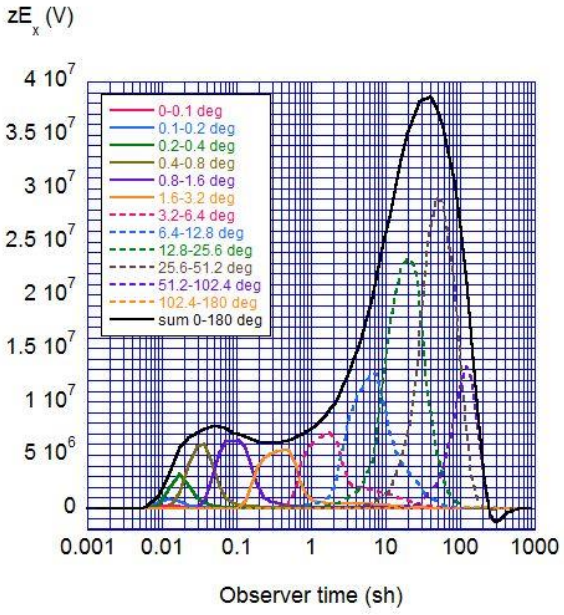

Figure 14. Field for a 0.1 sh conductivity ramp.

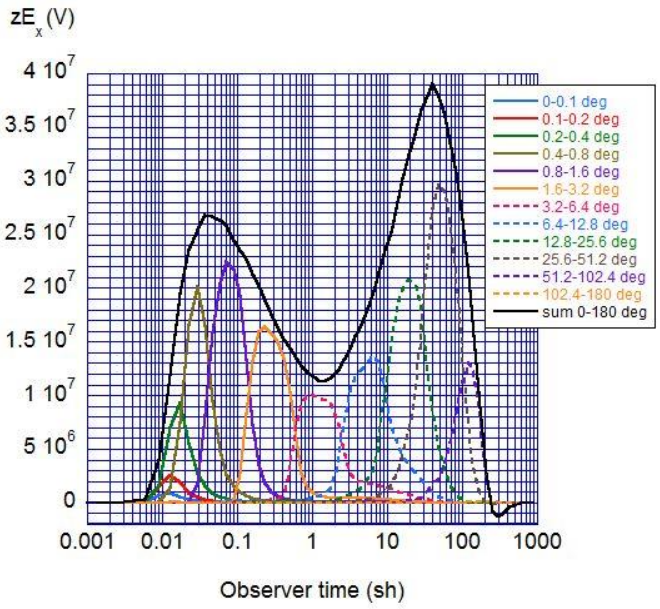

Figure 15. Field for a 0.5 sh conductivity ramp.

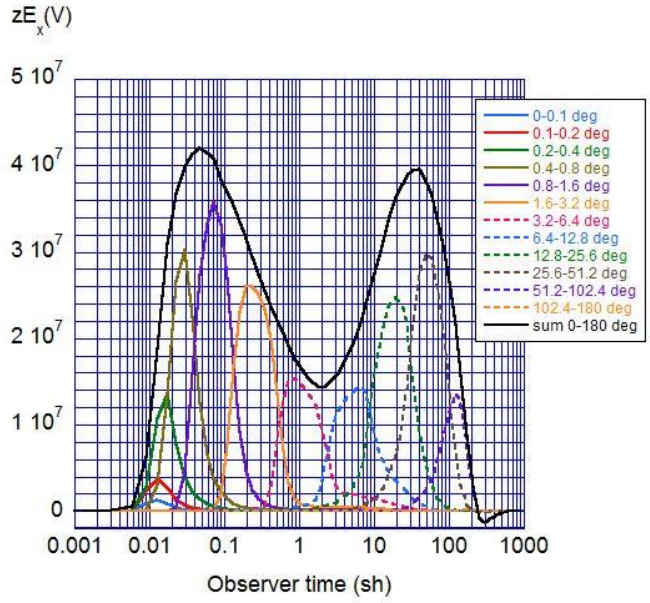

Figure 16. Field for a 1 sh conductivity ramp.

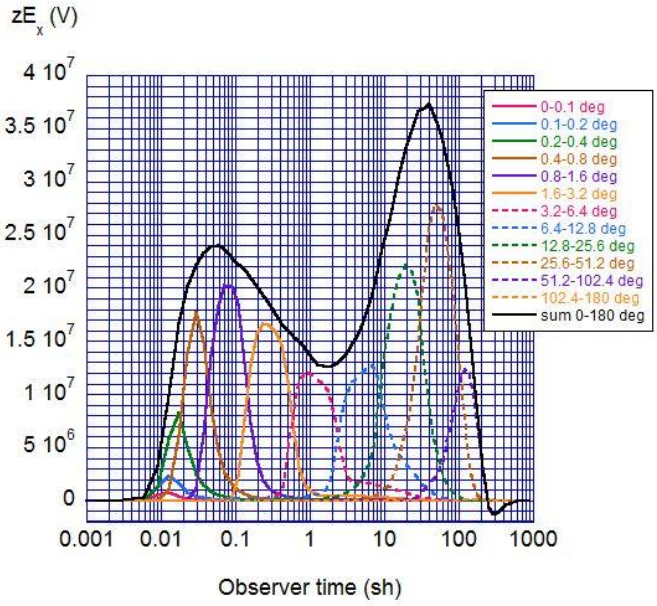

Figure 17. Field for the TDET conductivity model.

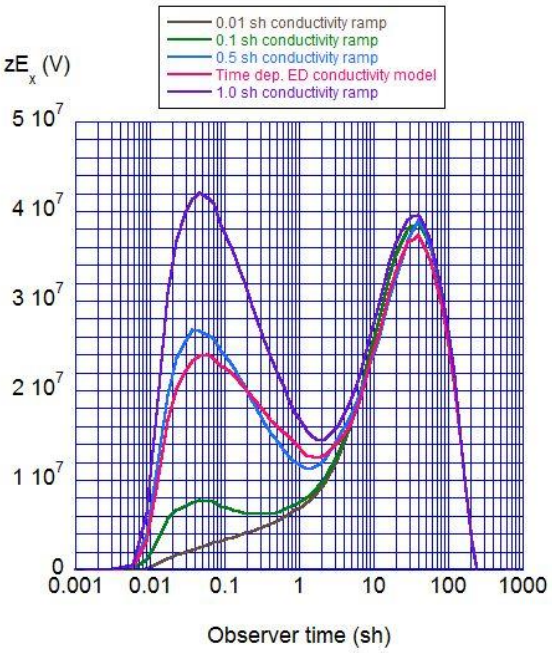

Figure 18. Fields for the indicated conductivity ramps and the TDET conductivity model.

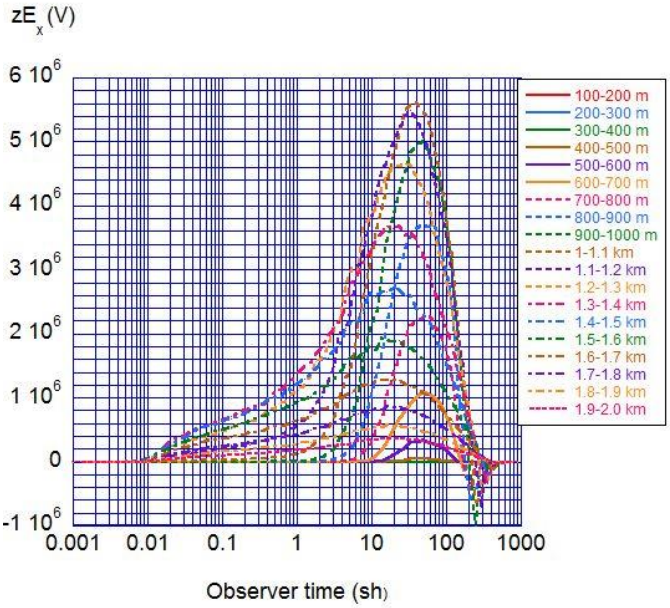

Figure 19. Contribution of indicated air shell to total field for 0.01 sh conductivity ramp.

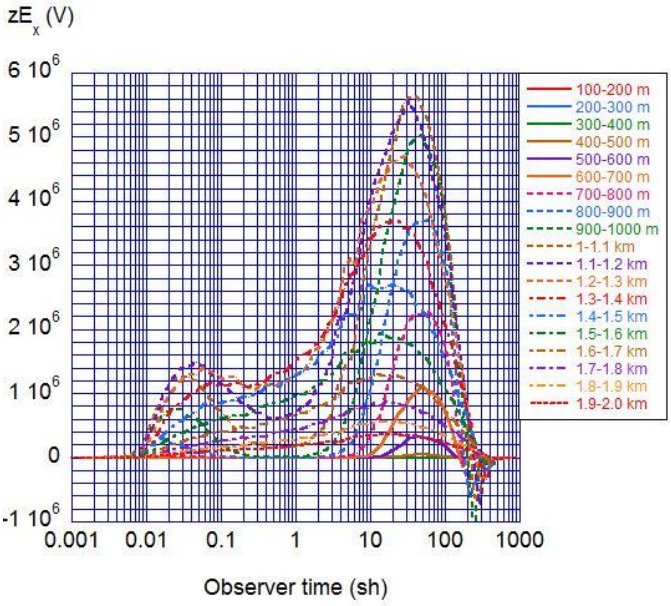

Figure 20. Contribution of indicated air shell to total field for 0.1 sh conductivity ramp.

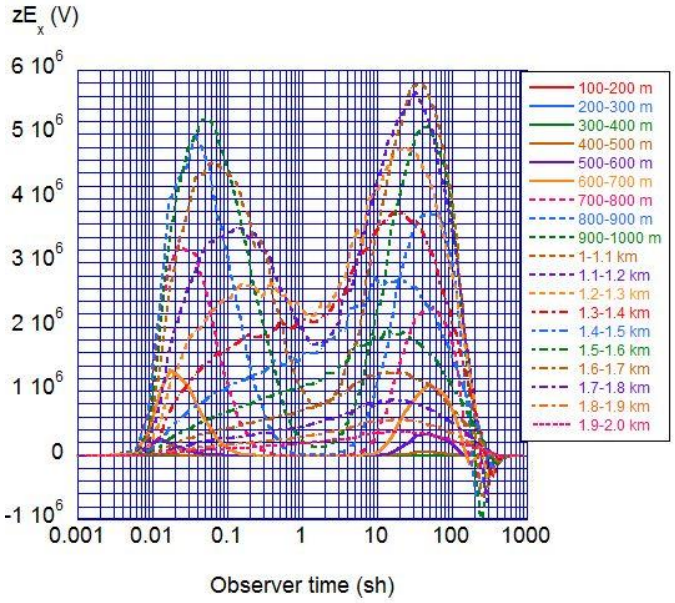

Figure 21. Contribution of indicated air shell to total field for 0.5 sh conductivity ramp.

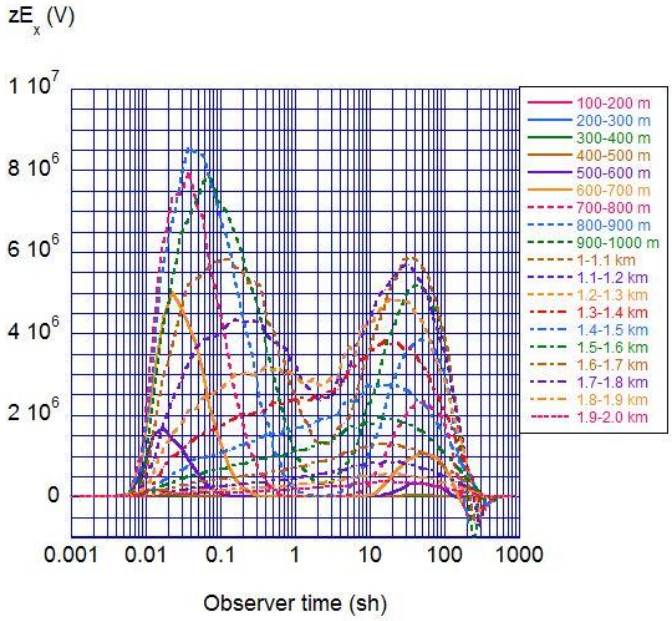

Figure 22. Contribution of indicated air shell to total field for 1 sh conductivity ramp.

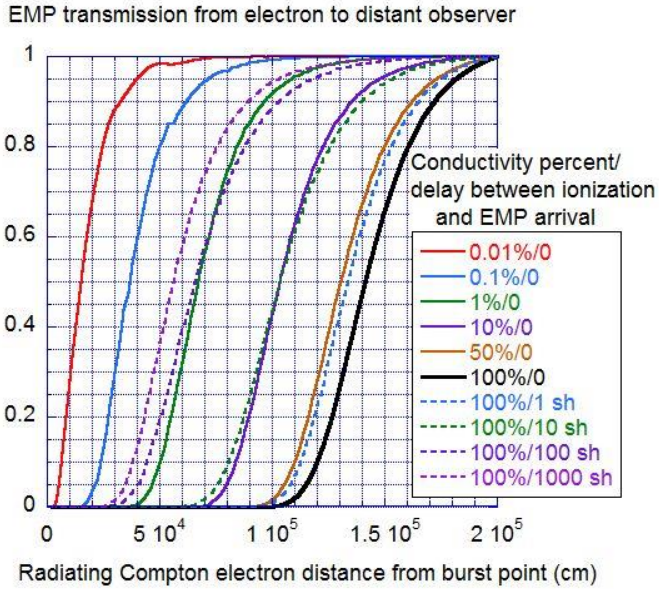

Figure 23. EMP transmission to a distant observer from radiating electrons located a given distance from the burst point for the indicated percent of conductivity and delay. Total yield 1 kt, 0.3% gammas, 3 Mev gamma energy. Sea level burst.

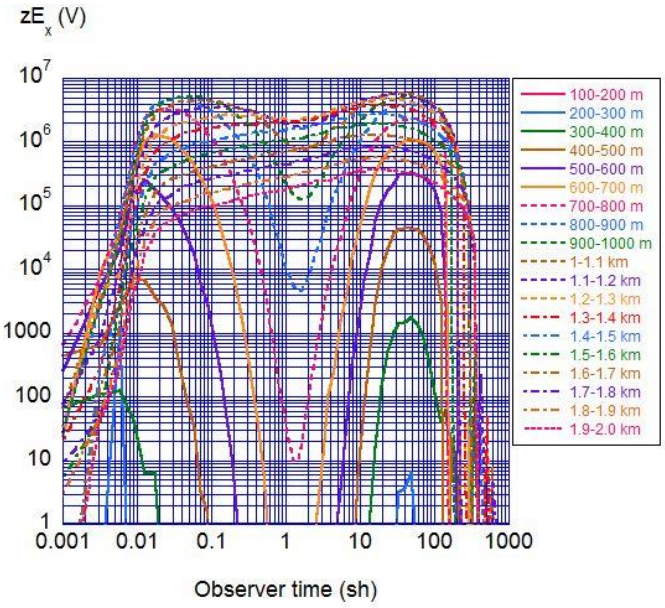

Figure 24. Field for 0.5 sh conductivity ramp and 3D conductivity model.

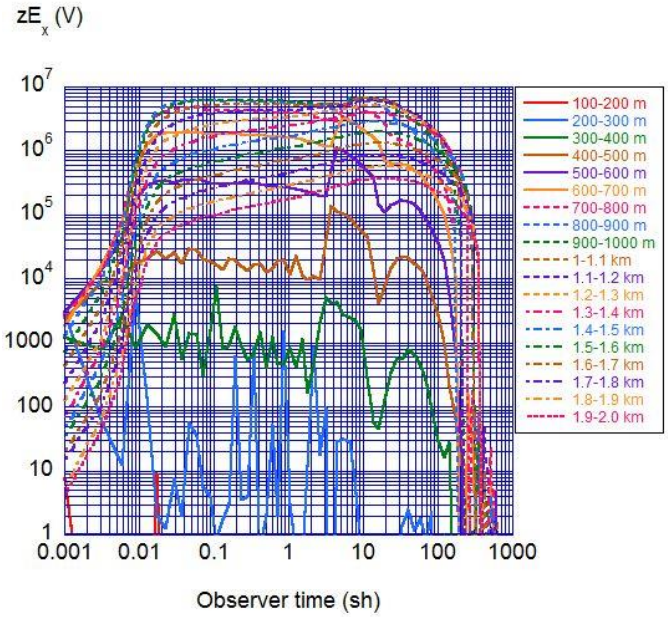

Figure 25. Field for 0.5 sh conductivity ramp and 1D conductivity model.

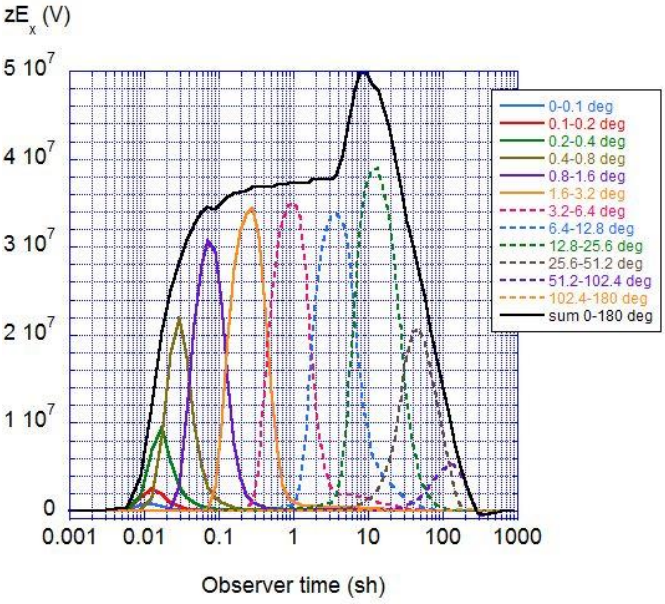

Figure 26. Total field for a 0.5 sh conductivity ramp and the 1D conductivity model.

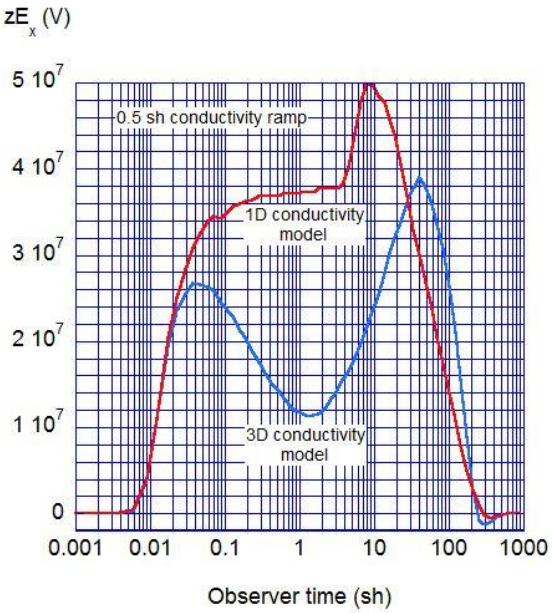

Figure 27. Overlay of the total fields for the 1D and 3D conductivity models (0.5 sh conductivity ramp).

External distribution

Eric Nelson (LANL)

Tim Goorley (LANL)

Xuan-Min Shao (LANL)

Randy Bos (LANL)

Morrie Pomgratz (LANL)

Tess Light (LANL)

Laurie Triplet (LANL)

Phil Dreike (SNLL)

Bruce Wilson (DTRA)

Lisa Andivahis (DTRA)

Heather Jiles (DTRA)

Mike Roony (DTRA)

Joan Pierre (DTRA)

Mike Frankel (DTRA contractor)

Jonathan Morrow-Jones (ARA)

Erin Lenon (ARA)

Bill Crevier (ARA)

Bernie Roth (ARA)

Steve Moosman (AFTAC)

John Carson (AFTAC)

Marvin Fransden (AFTAC)

Robert Roussel-Dupre (AFTAC contractor)

Robert Wiley (AFTAC contractor)

Dan Baker (U. Colorado/Boulder and AFTAC consultant)

George Carpenter (AFTAC consultant)

Anthony Clarke (AWE/UK)

LLNL internal distribution

David Larson

Chester Eng

Will Farmer

Bruce Cohen

Alex Friedman

Dave Grote

David Simons

Tom Carey

Ron Soltz

Bob Kirkwood

Scott Wilks

Barry Kirkendall

Paul Miller

Richard Ward